https://doi.org/10.1016/j.buildenv.2016.12.001

Model development of heat/mass transfer for internally cooled dehumidifier concerning liquid film shrinkage shape and contact angles

Chuanshuai Dong [a], Lin Lu [a, *], Ronghui Qi [a, b]

[a] Department of Building Services Engineering, The Hong Kong Polytechnic University, Kowloon, Hong Kong SAR, China

[b] School of Chemistry and Chemical Engineering, South China University of Technology, Guangzhou, China

[*] *Corresponding email: vivien.lu@polyu.edu.hk*

Tel.: +852 3400 3596; fax: +852 2774 6146.

Abstract

Moisture affects building materials, the thermal comfort of building occupants and the work performed by them. The plate liquid desiccant air-conditioning system (LDACS) is a promising dehumidification alternative to traditional air-conditioning system for lower energy consumption and less pollution. The shrinkage of the falling film on working plates critically influences the dehumidification performance by affecting the wetting area and film thickness. This paper developed a new model of plate dehumidifier concerning the shrinkage shape and the variable film thickness of falling film. The new model was validated by experiments and compared with existing models. The results indicated that the effect of contact angles on dehumidification performance can be accurately predicted. The moisture removal rates increased rapidly from 2.0 g/kg to 2.56 g/kg as the contact angles decreased from 85° to 5°, while the wetting area increased from 0.145m^2 to 0.176m^2. The distribution of the humidity ratio of process air along flow direction with different contact angles was also simulated. Besides, the average film thickness decreased from 0.952mm to 0.889mm as the contact angles decreased from 85° to 5°. The annual electricity consumption of plate LDACS with different contact angles for a typical building in Hong Kong was estimated and analysed by using the newly developed model. The new model can achieve a better predictive accuracy by considering the exact shrinkage shape of falling film and the findings can provide a new insights improving the performance of plate dehumidifiers and other industrial applications, such as vertical condensers, evaporators and absorption towers.

Keywords: liquid desiccant air-conditioning system; contact angle; shrinkage shape; wetting area; dehumidification performance

Nomenclature

A	Wetting area	m^2	α	Contact angle	°
CA	Contact angle	°	β	Shrinkage angle	°
C_p	Specific heat	kJ/(kg·K)	γ	Latent heat	kJ/kg
d	Width of the air channel	m	ω	Humidity ratio	g/kg
D	Width of the rim part	m	$\Delta\omega$	Moisture removal rate	g/kg
h	Enthalpy	kJ/kg	σ	Surface tension	N/m
h_c	Heat transfer coefficient between air and desiccant	W/(kg·K)	ε	Deformation factor	
h_d	Mass transfer coefficient	kg/(m^2·s)	ρ	Density	kg/m^3
h_f	Heat transfer coefficient between cooling water and desiccant	W/(kg·K)	δ	Film thickness	mm
H	Height	m	μ	Dynamic viscosity	Pa·s
k	Mass diffusion coefficient	m^2/s	***Subscripts***		
L	Length	m	*ave*	Average	
Le	Lewis number		*cen*	Central part	
m	Mass flow rate	kg/s	*f*	Cooling water	
n	Element number		*g, G*	Air	
P_0	Base value		*L*	Liquid solution	
Δp	Variation		*m*	Maximum	
Re	Reynolds number		*rim*	Rim part	
Sc	Schmidt number		*s*	Solution	
SC	Sensitivity coefficient		*S*	Solid	
T	Temperature	℃	*Sat*	Saturation status	
V	Velocity	m/s	*v*	Vapour	
W	Width	m	*x*	x coordinate	
Δx	Shrinkage distance	m	*y*	y coordinate	
X	Concentration	%	*z*	z coordinate	

1. Introduction

Liquid desiccant air-conditioning systems (LDACS) have drawn increasing attentions as possible alternative to the traditional vapour-compression refrigeration systems which have the limitations of high energy consumption, poor humidity control and low indoor air quality [1]. By handling the extra humidity with liquid desiccant absorption, the LDACS are energy-efficient and environment-friendly, especially in hot and humid regions. Furthermore, low-grade energy, such as solar energy or industrial waste energy, can be used in the regenerators of LDACS [2], which helps further reduce the system energy consumption. In principle, the hybrid

system combining liquid desiccant units and traditional vapour-compression chilling units can achieve a marked increase in the coefficient of performance (COP) [3, 4].

LDACS with packing dehumidifiers/regenerators are widely used and featured by large contact area between the liquid desiccant and the process air [5-10]. However, there occurs some problems, such as high air pressure loss and carryover of desiccant droplets. Droplet carryover can cause the corrosion of the ventilation system and the potential pollution of indoor air [11]. Plate LDACS with internally cooled/ heated units are developed to solve these two problems. The latent heat released during the absorption process is removed simultaneously by the internally-cooled unit to avoid temperature increase of liquid desiccant. Therefore, a relatively low surface vapour pressure can be maintained, which facilitates the mass transfer between liquid desiccant and process air [12]. Many researchers investigated the heat and mass transfer performance of plate LDACS [13-18]. Zhang et al. [19] analysed the operating performance of an internally-cooled dehumidifier experimentally and theoretically. Yin et al. [20] investigated the internally cooled/heated dehumidifier/regenerator of liquid desiccant systems experimentally, and found that the regeneration efficiency of internally heated regeneration was much higher than that of the adiabatic one. In addition, several simulation models including the finite differential model [21, 22], effectiveness-NTU model [23] and various simplified models [24], are available to predict the heat and mass transfer performance of LDACS. Niu [25] developed a two dimensional (2-D) model based on the finite differential model to investigate the performance of dehumidifiers, in which the mass transfer coefficient was obtained from experiments. Moreover, Ren [23] proposed corrections to the simple effectiveness-NTU method for counter-flow cooling towers. Liu et al. [26] developed a simplified method using enthalpy effectiveness and moisture effectiveness as indexes to predict dehumidifier performance. Three types of models for internally cooled/heated dehumidifier/regenerator were summarized by Luo et al. [16], i.e., models not considering the liquid film thickness, models considering uniform liquid film thickness and models considering variable liquid film thickness.

The wetting area of the liquid desiccant is a critical factor affecting the dehumidification performance of LDACS [27]. Many researchers have investigated the uncomplete wetting characteristics of falling film [28, 29]. Peng and Howell [30] theoretically investigated the incomplete surface wetting conditions in desiccant air conditioners. Jain et al. [31] subsequently proposed two wetness factors to investigate the influence of incomplete wetting on heat and mass transfer performance. Zhang et al. [32] experimentally investigated the shrinkage characteristics of heated falling film over a vertical stainless steel plate, and observed a pronounced contraction of the falling film along the flow direction caused by Marangoni effect.

Generally, the incomplete wetting characteristics, especially the exact shrinkage shape of the falling film, have not been taken into consideration in most of the simulation models. In addition, the variation of the falling film thickness along the flow direction has seldom been considered. In this paper, a new model of internally cooled dehumidifier considering the falling film shape and variable film thickness with different contact angles was developed to estimate the dehumidification performance. As the contact angle of the liquid on the working surface can significantly affect the wetting area of falling film [33], a comparative experimental setup of plate dehumidifiers with different working plates was also conducted. The new model was validated by the experimental results and compared with the existing models. The effect of contact angles on dehumidification performance as well as wetting area and falling film thickness was investigated theoretically. Then the effect of the desiccant solution temperature and cooling water temperature on the wetting area with different contact angles was also investigated. Lastly, the annual electricity consumption of plate LDACS with different contact angles for a typical commercial building in Hong Kong was estimated and analysed using the newly developed model.

2. Methodology

In this paper, both experimental and simulation studies were carried out to investigate the wetting area and heat/mass transfer performance of plate dehumidifiers with different surface contact angles.

2.1 Model development of falling film shrinkage with different contact angles

According to Zhang et al. [32] and our previous research [33], the falling film shrinks rapidly along the flow direction and the shrinkage varies considerably depending on the contact angles of the desiccant solution on working surface. In this study, the model was extended to very low contact angles of around 10°, which can be achieved with super-hydrophilic coating. As shown in Fig. 1 (a), the falling film can be divided into two parts, i.e., the central part and the rim part. The shrinkage is caused by the surface tension gradient between these parts.

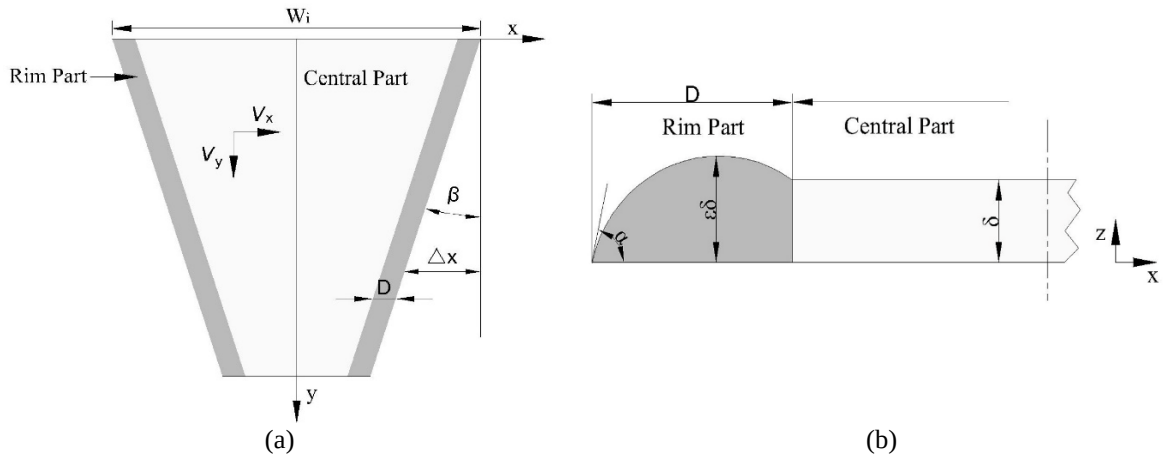

Fig. 1. Schematic of (a) falling film and (b) rim part

The shrinkage width Δx can be calculated from the velocity component in the transverse direction V_x. The transverse velocity component can be obtained by the momentum equation in the rim part:

$$\mu_s \frac{\partial^2 V_x}{\partial z^2} = 0 \tag{1}$$

where μ_s is the dynamic viscosity of the desiccant solution. The boundary conditions can be calculated as below:

$$z = 0,\ V_x = 0; \qquad z = \delta,\ \mu_s \frac{\partial V_x}{\partial z} = \frac{\partial \sigma}{\partial x}\cos\beta$$

where σ is the surface tension of the desiccant solution, and β, as shown in Fig. 1(b), is the angle between the shrinkage line and the *y*-axis, which can be calculated as below:

$$\beta = \frac{V_{y,m}}{\sqrt{V_{y,m}^2 + V_x^2}} \tag{2}$$

δ is the thickness of the falling film, which can be calculated as below:

$$\delta = \left(\frac{3 m_s \mu_s}{W(y) \rho_s^2 g} \right)^{1/3} \tag{3}$$

where $W(y)$ represents the width of the falling film at a given position on the *y*-axis.

Therefore, by combining the equations above, the transverse velocity V_x can be expressed as below:

$$V_x = \frac{\sqrt{2}}{2} V_{y,m} [(1 + \frac{4(\frac{\delta(\sigma_{cen} - \sigma_{rim})}{4\mu_s D})^2}{V_{y,m}^2})^{0.5} - 1]^{0.5} \tag{4}$$

where σ_{cen} and σ_{rim} refer to the surface tensions of the desiccant solution at the central part and the rim part, respectively. The surface tension of LiCl was taken from Conde [34]. In Equations (2) and (4), $V_{y,m}$ stands for the maximum velocity of the falling film at the y-axis, which can be calculated by Equation (5):

$$V_{y,m} = \frac{1}{2} \frac{\rho_s g}{\mu_s} \delta^2 \tag{5}$$

In Equation (4), D stands for the width of the rim part, as shown in Fig. 1(b). By geometrical analysis, the value of D can be obtained as below [32]:

$$D = \frac{\varepsilon \delta \sin\alpha}{(1 - \cos\alpha)} + \delta \sqrt{\frac{2\varepsilon}{(1 - \cos\alpha)} (\varepsilon - 1) - (\varepsilon - 1)^2} \tag{6}$$

where ε is a deformation factor, which is related to the physical properties and the flow rate of the desiccant solution as well as the temperature difference between the desiccant solution and the working surface.

As the falling film flows down along the y-axis in the plate dehumidifier, the shrinkage width Δx at the y_0 position on the y-axis can be obtained by integrating the transverse velocity from the top of the falling film to the y_0 position:

$$\Delta x = \int_0^{y_0/V_{y,m}} V_x dt = \frac{\sqrt{2}}{2} V_{y,m} \frac{|\sigma_{rim} - \sigma_{cen}|}{\sigma_{rim} - \sigma_{cen}} \int_0^{y_0} [(1 + \frac{\delta^2 (\sigma_{rim} - \sigma_{cen})^2}{4 V_{y,m}{}^2 \mu_s^2 D^2})^{0.5} - 1]^{0.5} dy \tag{7}$$

Then, the wetting length at the y_0 position is calculated as below:

$$W_{y_0} = W_i - 2\Delta x = W_i - \sqrt{2} V_{y,m} \frac{|\sigma_{rim} - \sigma_{cen}|}{\sigma_{rim} - \sigma_{cen}} \int_0^{y_0} [(1 + \frac{\delta^2 (\sigma_{rim} - \sigma_{cen})^2}{4 V_{y,m}{}^2 \mu_s^2 D^2})^{0.5} - 1]^{0.5} dy \tag{8}$$

where W_i is the initial wetting length at the inlet of the plate dehumidifier.

Finally, the total wetting area of the falling film can be calculated by integrating the wetting length from the top to the bottom:

$$A = \int_0^H W(y) dy \tag{9}$$

where A is the total wetting area of the desiccant solution and H is the height of the working plate.

2.2 Model development of heat and mass transfer with variable film thickness in internally cooled plate dehumidifier

Fig. 2 shows the schematic of the internally cooled plate dehumidifier. Heat and mass transfer occur between the upward-flowing air and downward-flowing desiccant solution in Channel I, while the latent heat released during the absorption process is removed by the cooling water in Channel II, which prevents the temperature increase of the desiccant solution. Therefore, the driving force of moisture exchange can be maintained large.

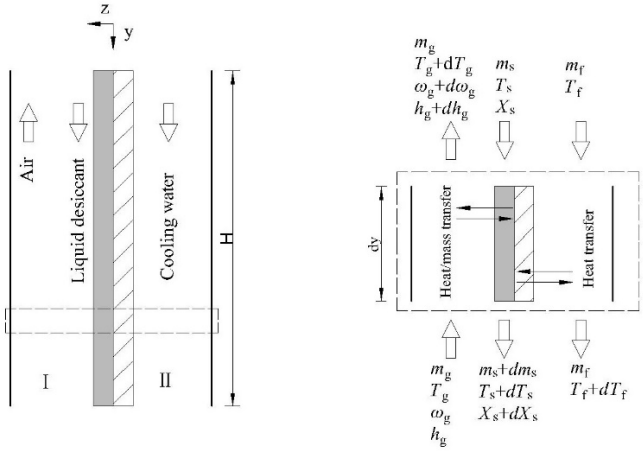

Fig. 2. Schematic of the internally cooled plate dehumidifier

To simplify the heat and mass transfer model of the internally cooled plate dehumidifier, several assumptions were made in the present model:

(1) The properties of the desiccant solution, air and cooling water are considered constant within the control volume.

(2) The desiccant solution, air and cooling water are considered well mixed in the cross-section.

(3) The plate dehumidifier is assumed to be well insulated and adiabatic.

(4) The local wall temperature is assumed equal to the local cooling water temperature due to the high heat conductivity of the working plate.

A control volume with the width of d*y*, as shown in Fig. 2, is presented to illustrate the heat and mass transfer in the plate dehumidifier. The mass and energy balance equations of the control volume are listed below.

The heat transfer equation between air and desiccant solution is described by:

$$m_g C_{pg} dT_g = h_c (T_s - T_g) W(y) dy \tag{10}$$

The mass conservation equation of air is described by:

$$m_g d\omega_g = dm_s = h_d (\omega_{sat} - \omega_g) W(y) dy \tag{11}$$

The energy conservation equation of air is described by:

$$dh_g = (C_{pg} + C_{pv}\omega_g) dT_g + (\gamma + C_{pv} T_g) d\omega_g \tag{12}$$

The energy conservation equation of the desiccant solution is described by:

$$m_f C_{pf} dT_f + d(m_s h_s) + m_g dh_g = 0 \tag{13}$$

where $d(m_s h_s)$ can be calculated as below.

$$d(m_s h_s) = m_s dh_s + h_s dm_s = m_s C_{p,s} dT_s + h_s dm_s \tag{14}$$

Therefore, the energy conservation equation of the desiccant solution can be rewritten as below:

$$dT_s = -\frac{1}{C_{ps}} \left(\frac{m_g}{m_s} dh_g + \frac{m_g}{m_s} C_{ps} T_s d\omega_g + \frac{m_f}{m_s} C_{pf} dT_f \right) \tag{15}$$

The mass conservation equation of the desiccant solution is described by:

$$dX_s = \frac{-dm_s}{m_s - m_g d\omega_g} X_s \tag{16}$$

The energy conservation equation of the cooling water is described by:

$$m_f C_{pf} dT_f = h_f (T_s - T_w) W(y) dz \tag{17}$$

In the above equations, ω_{sat} is the moisture content of the air which is in equilibrium with the desiccant solution and h_f represents the overall heat transfer coefficient between the cooling water and the desiccant

solution. h_c and h_d refer to the heat and mass transfer coefficients between the process air and the desiccant solution, respectively. The relationship between h_c and h_d is expressed as below:

$$Le = \frac{h_c}{h_d C_{pg}} \tag{18}$$

where Le is Lewis number. In present model, the mass transfer coefficient is calculated as below [35]:

$$h_{d.} = \frac{0.345 T_s^{-2.991} Re^{1.56} Sc^{0.33} k}{d} \tag{19}$$

where k represents the mass diffusion coefficient and d the width of the air channel.

The finite difference method (FDM) is adopted to solve the equations in the present model. As shown in Fig. 3, the plate dehumidifier can be divided into *n* differential elements with variable wetting lengths. $W(y)$ is the actual wetting length of the falling film. For each differential element, $W(y)$ must be calculated again based on the local flow parameters. In the new model, the film thickness is assumed to be variable along the flow direction. As the film thickness is related with $W(y)$ (Equation 3, 6, 8), iteration is adopted in the calculation process.

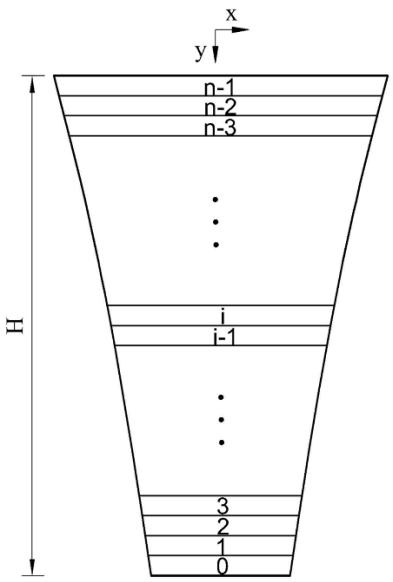

Fig. 3. Numerical model of plate dehumidifier with variable wetting length

2.3 Experimental setup of plate dehumidifiers

An experimental setup with two comparative channels, as shown in Fig. 4, was constructed to investigate the influence of the surface contact angle on the wetting area in plate dehumidifiers. The experimental setup contains four main parts, i.e., the plate dehumidifiers, the liquid desiccant loop, the air loop and the cooling water loop. The plate dehumidifiers were composed of two comparative channels with dimensions of 550×100×600mm ($L \times W \times H$). Steel plates were chosen as the working surface for each channel, respectively. In Channel I, the

steel plate was cleaned with ethanol, while in Channel II, the steel plate was coated with super-hydrophilic coating to obtain lower contact angles. The contact angles of deionized water and LiCl aqueous solution with 38% in mass concentration are shown in Fig. 5. The contact angles of deionized water and LiCl aqueous solution on uncoated steel plate were 82.5° and 84.6°, respectively. However, the contact angles on steel plates with super-hydrophilic coating were significantly reduced to 12.9° and 15.7°. A thermal image camera was used to capture images of the falling film in the plate dehumidifier with different contact angles. In the liquid desiccant loop, the liquid desiccant was pumped from the storage tank to the top of the plate dehumidifier. The even distribution of the falling film was achieved by liquid distributors. Then, the liquid desiccant came into contact with the upward-flowing humid air and returned to the storage tank. In the air loop, the air was supplied by fans. The temperature and humid ratio of the circulated air were controlled by operating the air heater and the electrode humidifier installed at the inlet of the plate dehumidifier. Heat and mass transfer occurred between the air and the desiccant solution. Cooling water circulated around the back of the working plate to remove the latent heat released during the absorption process. In addition, the experimental setup was insulated with neoprene foam to reduce the influence of the surroundings.

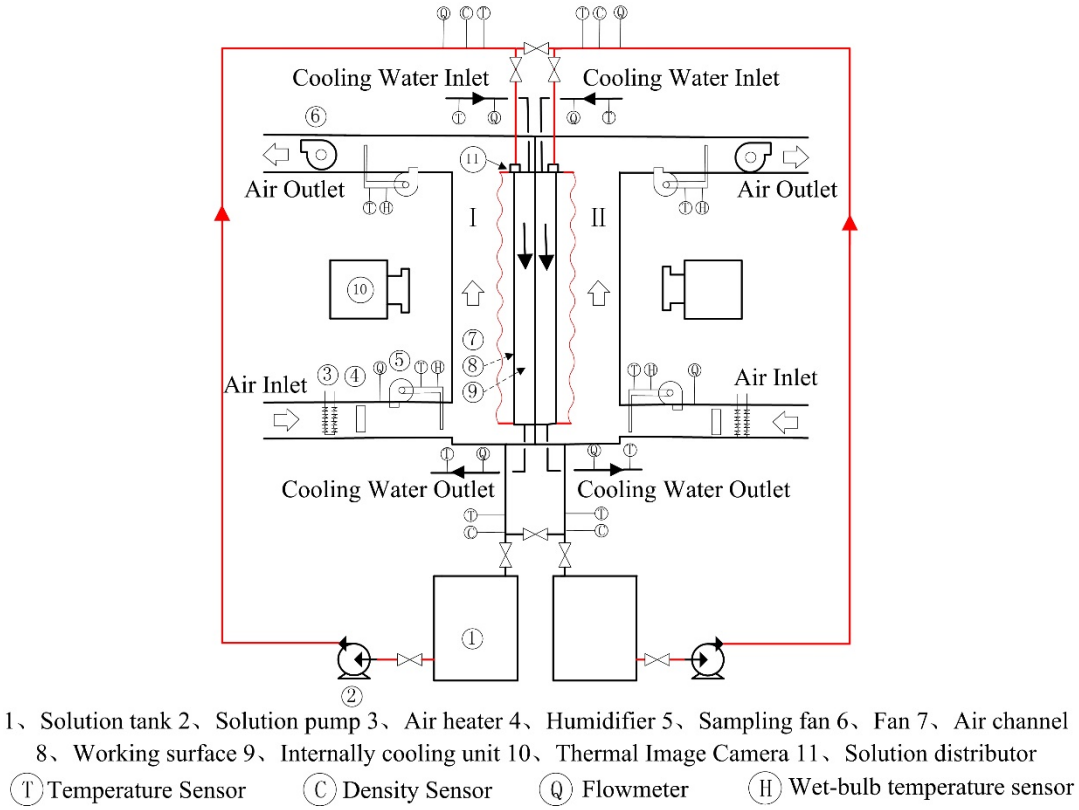

Fig. 4. Schematic of experimental setup

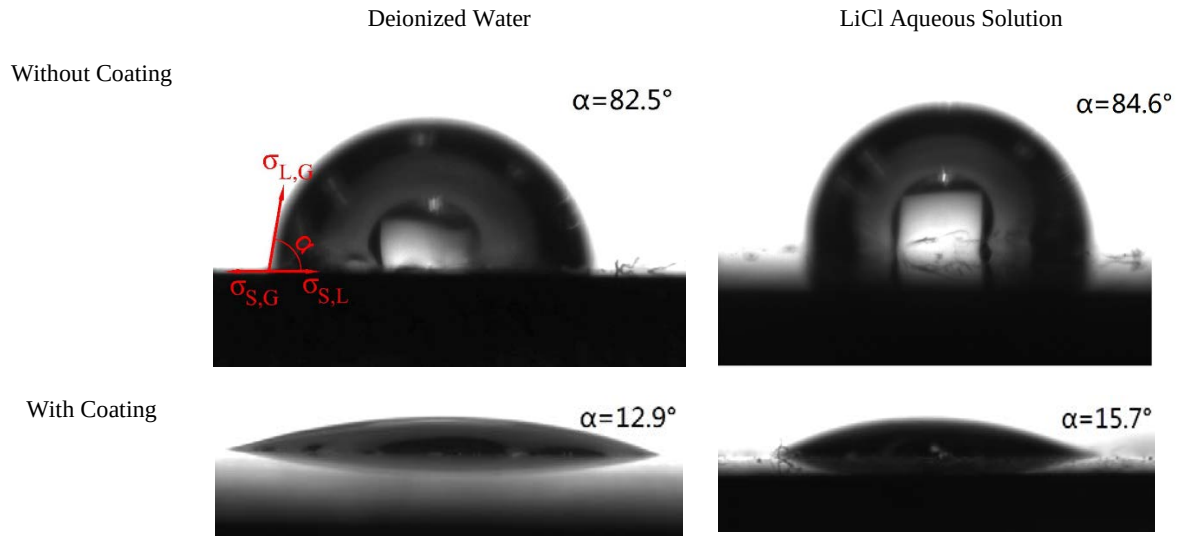

Fig. 5. Contact angles of deionized water and LiCl aqueous solution on steel plate with and without super-hydrophilic coating

3. Results and discussion

3.1 Results validation

To validate the new dehumidification model with variable wetting length, the simulation results were compared with the existing experimental results [36]. The uncertainties of the experimental results were 8.32%. The Average Relative Deviation (*ARD*) between the simulation and the experimental results was proposed as below:

$$ARD = \frac{1}{num}\sum_{i=1}^{num}\left|\frac{\varepsilon_{\mathrm{exp,i}} - \varepsilon_{\mathrm{cal,i}}}{\varepsilon_{\mathrm{exp,i}}}\right| \times 100\% \tag{26}$$

where *num* is the number of simulation results.

Fig. 6 demonstrates the comparison of the simulation moisture removal rates and the experimental results. All of the simulation results fell within the $\pm 10\%$ error band of the experimental results with an *ARD* of 4.04%, which proves that the simulation results are reliable.

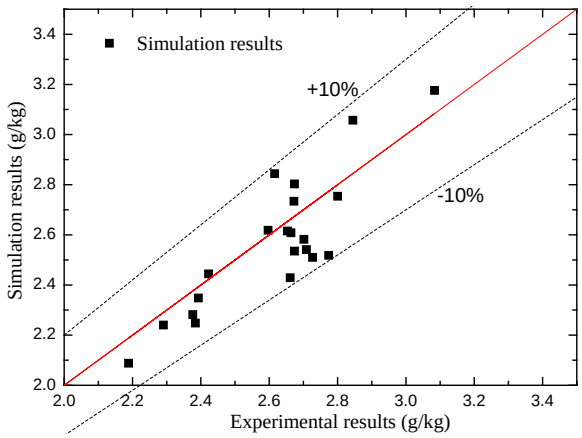

Fig. 6. Comparison of the simulation results with the experimental data

The comparison of the simulated film boundaries with the corresponding experimental ones at different contact angles is presented in Fig. 7. The simulation results are in good agreement with the measured boundaries, which illustrates that the present new model can accurately predict the shrinkage of the falling film and the influence of contact angles on the shrinkage. In addition, it can be clearly observed that the shrinkage of the falling film is more pronounced with larger contact angles.

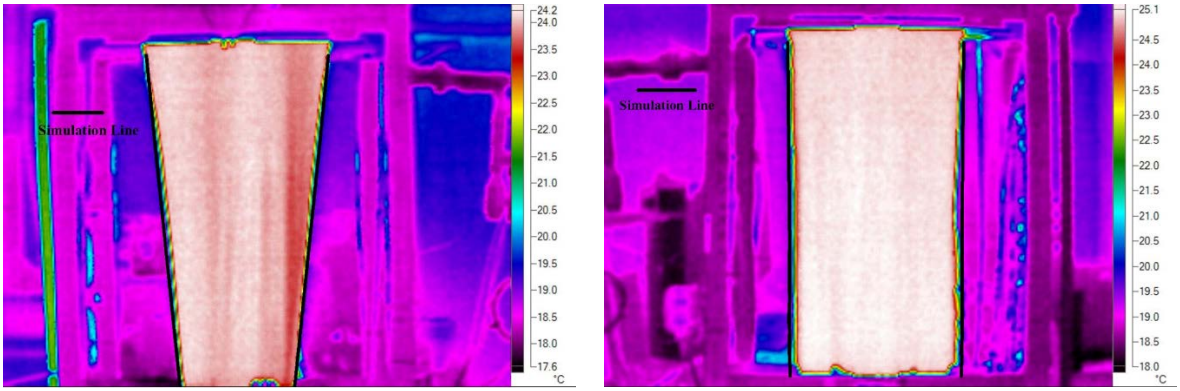

(a) (b)

Fig. 7. Comparison of the simulated and experimental film boundaries with different contact angles: (a) CA = 84.6° (b) CA = 15.7°

The simulation results of the outlet air humidity ratio by the present new model and the model developed by Yin et al [36] were compared and analysed, as shown in Fig. 8. The ARD between the simulation results of the two models were 3.7% and 4.71% for the contact angles of 5° and 85°, respectively. Interestingly, the outlet air humidity ratio calculated by the present model was slightly higher than that calculated by Yin et al. [36] and the difference was more pronounced with higher contact angles. In the new model, the wetting length was calculated based on the shrinkage of the falling film, while in the model of Yin et al. [36] this value was simply taken as the width of the working plate. Therefore, the moisture removal rate simulated by the new model was slightly lower than the results calculated that by Yin et al. [36] and the difference increased at higher contact angles, where the shrinkage of the falling film was greater.

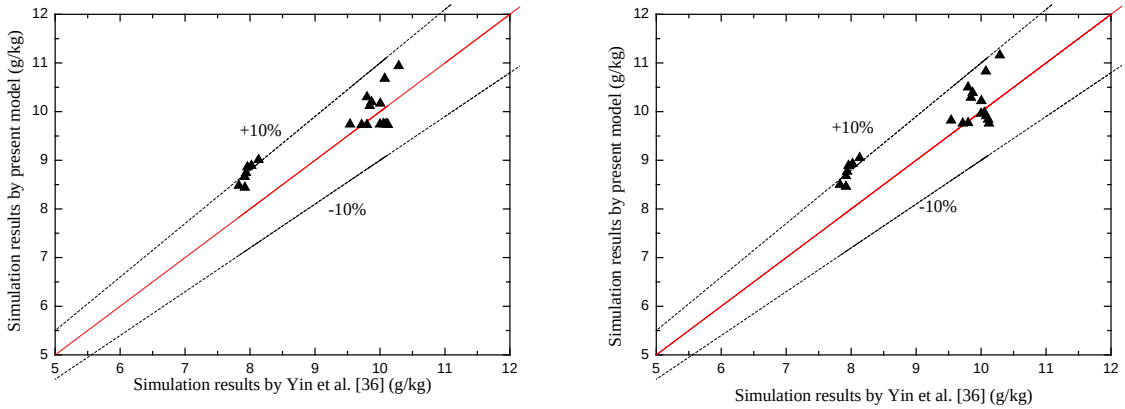

(a) CA=5° (b) CA=85°

Fig. 8. Comparison of the simulation results by the present model and Yin et al [36] model with different contact angles

To further validate the new model, uncertainty analysis was also conducted, as shown in Table 1. The outlet air humidity ratio was selected as the index in the analysis. In addition, a dimensionless sensitivity coefficient, *SC*, was introduced to investigate the influence of the input parameters on the outlet results [37]. *SC* can be obtained as below:

$$SC = \frac{\left|\omega_{p_0+\Delta p} - \omega_{p_0}\right| + \left|\omega_{p_0-\Delta p} - \omega_{p_0}\right|}{2\Delta p} \times \frac{p_0}{\omega_{p_0}} \tag{27}$$

where p_0 and Δp represent the base values and uncertainty of the input parameters, respectively. It can be inferred from the analysis that the simulation results were heavily affected by the inlet desiccant solution parameters, such as the temperature and concentration, and as well as the inlet air humidity ratio. In addition, as the contact angles of the desiccant solution on the working surfaces differed significantly among the various plates, the influence of the contact angles on the simulation results was also important despite the small sensitivity coefficient of the contact angle.

Table 1 Uncertainty and sensitivity analysis of the new model

Input parameters	T_g (℃)	ω_g (g/kg)	m_g (kg/s)	T_s (℃)	m_s (kg/s)	X (%)	T_f (℃)	CA (°)
Base values	31	15	0.09	25	0.15	38%	22	45
Input uncertainty	±10%	±10%	±10%	±10%	±10%	±5.3%	±10%	±10%
Results uncertainty	0.11%	8.7%	1.6%	10.6%	0.17%	2.17%	3.78%	0.27%
SC	0.009	0.861	0.170	1.102	0.017	0.456	0.073	0.025

3.2 Effect of contact angles on wetting area and film thickness

Fig. 9 plots the shrinkage of the falling film along the flow direction with different contact angles. It is apparent that the falling film contracts intensively and becomes very narrow with larger contact angles, but only shows very slight shrinkage with lower contact angles. As the contact angle decreases from 85° to 5°, the wetting length at the outlet of the plate dehumidifier increases from 0.193 m to 0.291 m with the same initial wetting length of 0.296 m at the inlet of the dehumidifier. It can be calculated that the total wetting area increases significantly from 0.145 m^2 to 0.176 m^2. This phenomenon can be explained by the fact that the surface tension gradient is reduced at lower contact angles. According to Young equation [38], the contact angle depends on the relationship between the solid–gas interfacial tension $\sigma_{S,G}$, solid–liquid interfacial tension $\sigma_{S,L}$ and liquid–gas interfacial tension $\sigma_{L,G}$, as follows: $\cos\alpha = (\sigma_{S,G} - \sigma_{S,L})/\sigma_{L,G}$. The decrease in the contact angles implies the decrease in the solid–liquid interfacial tension and reduces the contraction of the falling film. In addition, as the surface tension gradient $(\sigma_{cen} - \sigma_{rim})/D$ decreases with the increase of D, and D increases with the decrease of

the contact angles, the surface tension gradient decreases with the decrease of the contact angles and the Marangoni effect in the transverse direction becomes weaker accordingly.

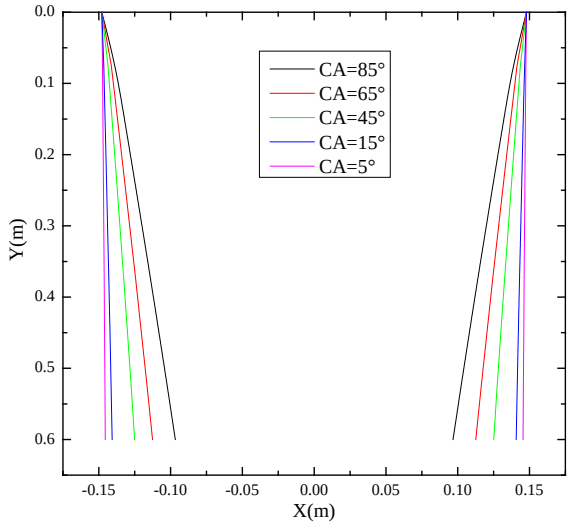

T_g (℃)	ω_g (g/kg)	m_g (kg/s)	T_s (℃)	m_s (kg/s)	X (%)	T_f (℃)
31	15	0.09	28	0.15	38.8	20

Fig. 9. Shrinkage of the falling film with different contact angles

Fig. 10 shows the variation of the wetting area with the desiccant solution temperature at different contact angles. It can be observed that the wetting area decreases with the increase of the desiccant solution temperature. As $T_{s,in}$ increases, the liquid falling film contracts and becomes narrower. This contraction occurs because the surface tension gradient in the transverse direction increases with the increase of the desiccant solution temperature and the shrinkage along the flow direction turns out more intensive. Another interesting finding is that the negative gradient differs considerably with the contact angle. The negative gradient decreases from 5.75×10^{-3} m^2/℃ with the contact angle of 85° to 0.27×10^{-3} m^2/℃ with the contact angle of 5°. A possible reason for this trend is that the width of the rim part, D, increases rapidly with the decrease of the contact angles which would weaken the effect of the desiccant solution temperature on the surface tension gradient. The effect of cooling water temperature on the wetting area at different contact angles is presented in Fig. 11, which resembles the trend for the desiccant solution temperature. The wetting area increases with the increase of cooling water temperature, but the rate of this increase depends on the contact angles. The positive gradient decreases from 4.67×10^{-3} m^2/℃ with the contact angle of 85° to 0.22×10^{-3} m^2/℃ with the contact angle of 5°, from which it can be inferred that increasing the cooling water temperature effectively reduces the surface tension gradient in the transverse direction at constant desiccant solution temperature.

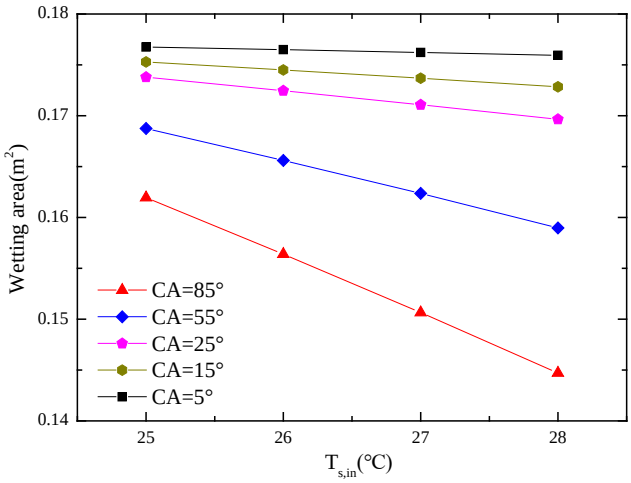

T_g (℃)	ω_g (g/kg)	m_g (kg/s)	$T_{s,in}$ (℃)	m_s (kg/s)	X (%)	T_f (℃)
31	15	0.09	25~28	0.15	38.8	20

Fig. 10. Effect of desiccant solution temperature on wetting area with different contact angles

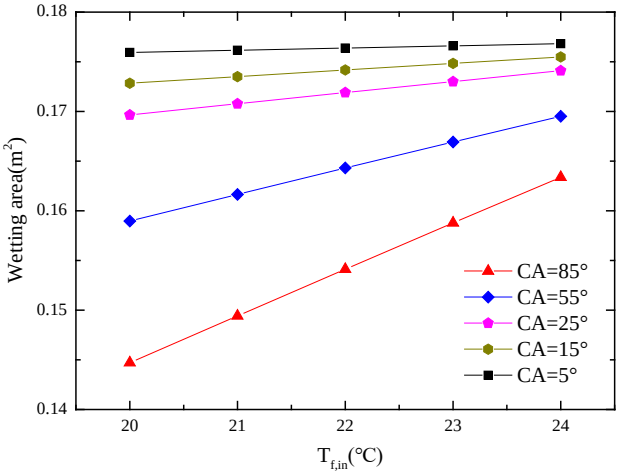

T_g (℃)	ω_g (g/kg)	m_g (kg/s)	$T_{s,in}$ (℃)	m_s (kg/s)	X (%)	T_f (℃)
31	15	0.09	28	0.15	38.8	20~24

Fig. 11. Effect of cooling water temperature on wetting area with different contact angles

Fig. 12(a) shows the variation of average falling film thickness with contact angles. The average falling film thickness is calculated based on the local falling film thickness at each differential element. It can be observed that the average falling film thickness $\delta_{s,ave}$ decreases rapidly from 0.952 mm to 0.889 mm as the contact angles decreases from 85° to 5°. This decrease occurs because of the marked increase in the wetting area at lower contact angles, as shown in Fig. 9. In addition, the distribution of the local falling film thickness along the flow direction with different contact angles is presented in Fig. 12(b). Y = 0 represents the inlet of the plate dehumidifier and Y = 0.6 m represents the outlet. It can be observed that the local falling film thickness increases along the flow direction. The falling film thickness is related to both the wetting length and the film velocity. On one hand, the wetting length is reduced along the flow direction, which acts to increase the falling film thickness. On the other hand, the film velocity increases along the flow direction, which acts, conversely, to thin the falling film. The

decrease of wetting length is more pronounced than the increase of film velocity, so the net effect is to increase the local falling film thickness. Another interesting observation in Fig. 12(b) is that the positive gradient of the local film thickness is determined by the contact angles. It can be observed that the positive gradient of local film thickness along the flow direction drops rapidly from 0.235mm/m to 0.0197mm/m as the contact angle decreases from 85° to 5°. Lower contact angles lead to reduced shrinkage of the falling film, which weaken the effect of the wetting length on the increase of film thickness.

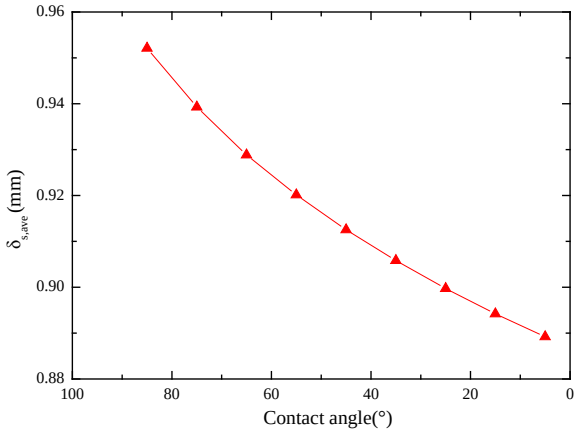

(a) Average falling film thickness

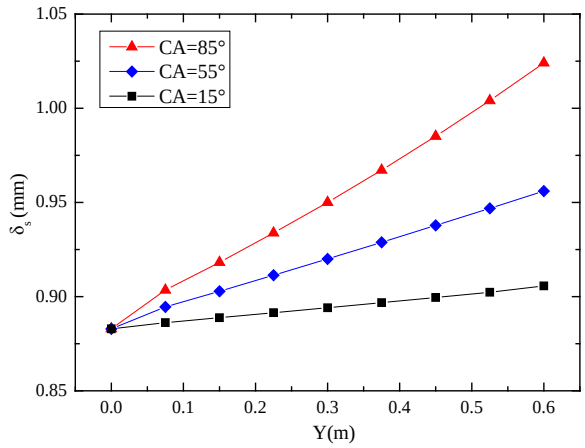

(b) Distribution of falling film thickness along the flow direction

T_g (℃)	ω_g (g/kg)	m_g (kg/s)	T_s (℃)	m_s (kg/s)	X (%)	T_f (℃)
31	15	0.09	28	0.15	38.8	20

Fig. 12. Variation of the falling film thickness with different contact angles

3.3 Effect of contact angles on the moisture removal rate

The variation of both the moisture removal rate and the ratio of the wetting area with contact angles are shown in Fig. 13. The ratio of the wetting area represents the ratio of the actual wetting area to the maximum wetting area of the plate dehumidifier. As the contact angle decreases from 85° to 5°, the moisture removal rate increases from 2.0 g/kg to 2.56 g/kg , i.e., by a factor of 1.28. Meanwhile, the ratio of the wetting area increases from 0.815 to 0.991, i.e., by a factor of 1.21. The increase in the wetting area effectively increases the contact area

between the desiccant solution and the process air, as well as increasing the moisture removal rate. Another interesting observation in Fig. 13 is that the increasing ratio of moisture removal rate is greater than that of the wetting area. One possible explanation for this is that at lower contact angles, the average falling film thickness is also lower, as shown in Fig. 12(a), which effectively reduces the heat transfer resistance between the cooling water and the desiccant solution and accelerates the replenishment of the superficial desiccant solution. Therefore, both the increase of the wetting area and the decrease of the falling film thickness benefit the heat and mass transfer performance of the internally cooled plate dehumidifier.

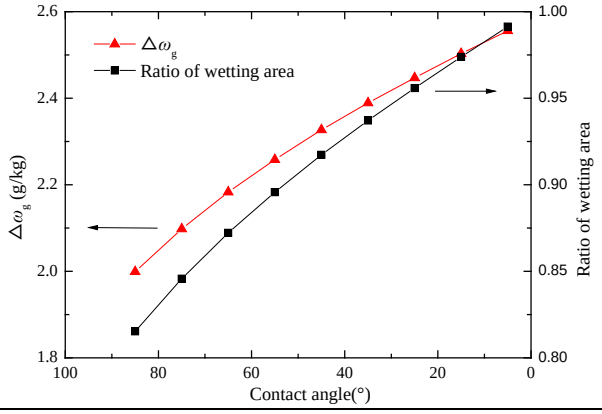

T_g (℃)	ω_g (g/kg)	m_g (kg/s)	T_s (℃)	m_s (kg/s)	X (%)	T_f (℃)
31	15	0.09	28	0.15	38.8	20

Fig. 13. Variation of moisture removal rate with contact angels

The effect of the desiccant solution temperature on the moisture removal rate with different contact angles is presented in Fig. 14. The moisture removal rate decreases rapidly with the increase of the desiccant temperature. This trend is related to the surface vapour pressure of the desiccant solution, which, at a given concertation, increases exponentially with the temperature. This in turn markedly reduces the driving force of mass transfer between the desiccant solution and the process air, thus significantly reducing the moisture removal rate at higher temperature. In addition, it can be observed in Fig. 14 that the effect of the contact angles on the moisture removal rate differs in desiccant solution temperature. As the contact angle decreases from 85° to 5°, the moisture removal rate at 25℃ increases from 3.43 g/kg to 3.78 g/kg , i.e., with an increment of 0.35 g/kg , whereas at 28℃ it increases from 2.0 g/kg to 2.56 g/kg , i.e., with an increment of 0.56 g/kg . One possible reason is that the effect of contact angles on wetting area is more intensive at higher desiccant solution temperature, as shown in Fig. 10, and therefore the contact angles shows bigger impact on heat and mass transfer at higher desiccant solution temperature.

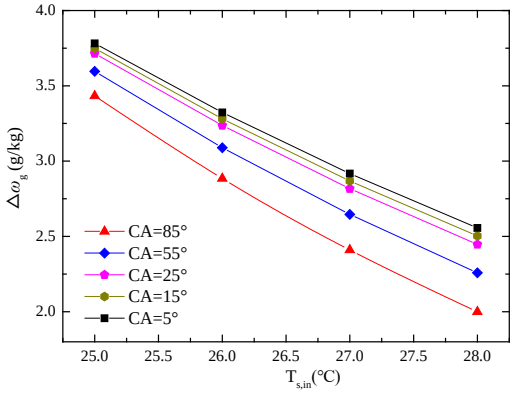

T_g (℃)	ω_g (g/kg)	m_g (kg/s)	T_s (℃)	m_s (kg/s)	X (%)	T_f (℃)
31	15	0.09	25~28	0.15	38.8	20

Fig. 14. Variation of moisture removal rate with desiccant solution temperature for different contact angles

Fig. 15 shows the distribution of the humidity ratio of the process air along the flow direction with different contact angles. Y = 0.6 m represents the inlet of the process air and Y = 0 represents the outlet. It can be observed that the humidity ratio decreases from the inlet to the outlet of the plate dehumidifier. The negative gradient increases with the decrease of the contact angles.

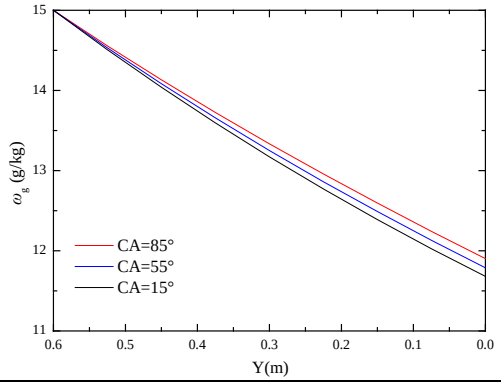

T_g (℃)	ω_g (g/kg)	m_g (kg/s)	T_s (℃)	m_s (kg/s)	X (%)	T_f (℃)
31	15	0.09	26	0.15	38.8	22

Fig. 15. Distribution of humidity ratio along the flow direction with different contact angles

3.4 Energy consumption of plate LDACS with different contact angles for a commercial building

A typical commercial building in Hong Kong was selected as a case building to estimate the energy consumption of LDACS with plate dehumidifiers and to investigate the effect of contact angles for the working plate on the energy consumption. The details of the buildings can be found in Qi [39]. The new model was applied in the system simulation process to estimate the moisture effectiveness and the enthalpy effectiveness of the plate dehumidifier with different contact angles. Fig. 16 shows the calculated annual electricity consumption of the LDACS with plate dehumidifier for contact angles of 84.6° and 15.7°. These contact angles are the previously measured values of LiCl aqueous solution on the raw steel plate and the coated steel plate with super-hydrophilic coating, respectively. As the contact angles decrease from 84.6° to 15.7°, the electricity of both the regenerator

and the chiller are reduced. Around 35 MWh of electricity could be saved per year of plate LDACS with lower contact angles by increasing the dehumidification performance.

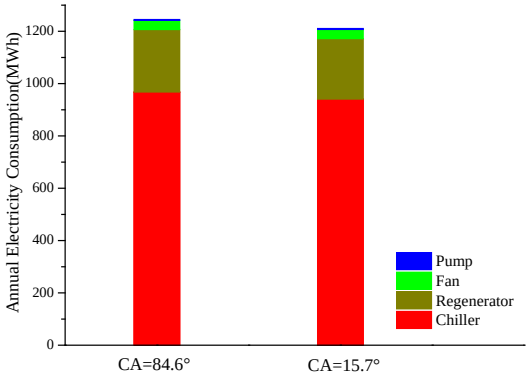

Fig. 16. Annual electricity consumption of plate LDACS with different contact angles

4. Conclusions

The shrinkage shape of falling film can critically influence the dehumidification performance of plate dehumidifier by affecting the wetting area and film thickness. The falling film shrinkage is mainly determined by the interaction between liquid desiccant and working surface at certain flow conditions. In present study, a new model of heat and mass transfer for the internally cooled/heated LDACS was developed concerning the shrinkage shape of falling film and the variable film thickness along the flow direction. In addition, a comparative experimental setup with different working plates was conducted to validate the new model.

The new model was validated by the experimental results and compared with the existing models. The effect of the contact angles for desiccant solution on moisture removal rates and wetting area can be effectively demonstrated in the new model. The results indicated that the moisture removal rate increased rapidly from 2.0 g/kg to 2.56 g/kg as the contact angles decreased from 85° to 5°, while the wetting area increased from 0.145 m^2 to 0.176 m^2. The effect of the desiccant solution temperature on the moisture removal rate and the wetting area with different contact angles was also investigated. Increasing the desiccant solution temperature sharply reduced the moisture removal rate and wetting area, but the decrement of both values was related with the contact angles. The distribution of the humidity ratio of the process air along the flow direction with different contact angles was also simulated. Further simulation results showed that the average film thickness decreased from 0.952 mm to 0.889 mm as the contact angles decreased from 85° to 5°. The distribution of the local film thickness along the flow direction was also simulated, and found to be significantly affected by the contact angles. In addition, the annual electricity consumption of plate LDACS for a commercial building in Hong Kong was estimated and analysed using the new model. Around 35 MWh of electricity can be saved per year with lower contact angles by increasing the dehumidification performance. By taking the shrinkage shape and variable thickness of falling film

into account, the new model can predict the performance of the plate dehumidifier more accurately. The findings can also applied in other industrial applications with liquid falling film, such as heat exchangers, vertical condensers, evaporators and absorption towers.

Acknowledgements

This work was supported by the RGC General Research Fund (PolyU 152010/15E) and The Hong Kong Polytechnic University through Central Research Grant (PolyU 152110/14E)

References

[1] Dai YJ. Wang RZ, Zhang HF, Yu JD. Use of liquid desiccant cooling to improve the performance of vapor compression air conditioning. Applied Thermal Engineering 2001; 21(12): 1185-1202.

[2] Pohl JP, Hellman HM, Grossman G. Investigation and comparison of two configurations of a novel open-cycle absorption chiller. International Journal of Refrigeration 1998; 21: 142-149.

[3] Liang CH, Zhang LZ, Pei LX. Independent air dehumidification with membrane-based total heat recovery: modelling and experimental validation. International Journal of Refrigeration 2010; 33(2): 398-408.

[4] Ge GM, Xiao F, Xu XH. Model-based optimal control of a dedicated outdoor air-chilled ceiling system using liquid desiccant and membrane-based total heat recovery. Applied Energy 2011; 88(11): 4180-4190.

[5] Zhang HJ, Liu JH, Zhang L. Experiment on mass transfer performance of a cross-flow dehumidifier. Journal of Refrigeration 2010; 31(6): 21-27.

[6] Longo GA, Gasparella A. Experimental and theoretical analysis of heat and mass transfer in a packed column dehumidifier/regenerator with liquid desiccant. International Journal of Heat and Mass Transfer 2005; 48: 5240-5254.

[7] Longo GA, Gasparella A. Experimental analysis on desiccant regeneration in a packed column with structured and random packing. Solar Energy 2009; 83: 511-521.

[8] Elsarrag E. Performance study on a structured packed liquid desiccant regenerator. Solar Energy 2006; 80: 1624-1631.

[9] Potnis SV, Lenz TG. Dimensionless mass-transfer correlations for packed bed liquid-desiccant contactors. Industrial & Engineering Chemistry Research 1996; 35: 4185-4193.

[10] Chung, TW, Gosh TK, Hines AL. Comparison between random and structured packings for dehumidification of air by lithium chloride solutions in a packed column and their heat and mass transfer correlations. Industrial & Engineering Chemistry Research 1996; 35(1): 192-198.

[11] Buker MS, Riffat SB. Recent developments in solar assisted liquid desiccant evaporative cooling technology-a review. Energy and Buildings 2015; 96: 95-108.

[12] Lowenstein AI, Gabruk RS. The effect of absorber design on the performance of a liquid desiccant air conditioner. ASHRAE Transactions 1992; 98(1): 712-720.

[13] Luo YM, Wang M, Yang HX, Lu Lin, Peng JQ. Experimental study of internally cooled liquid desiccant dehumidification: Application in Hong Kong and intensive analysis of influencing factors. Building and Environment, 2015; 93(2): 210-220.

[14] Gao WZ, Shi YR, Cheng YP, Sun WZ. Experimental study on partially internally cooled dehumidification in liquid desiccant air conditioning system. Energy and Buildings 2013; 61: 202-209.

[15] Gandhidasan P, Mohandes MA. Artificial neural network analysis of liquid desiccant dehumidification system. Energy 2011; 36:1180-1186.
[16] Luo YM, Yang HX, Lu L, Qi RH. A review of the mathematical models for predicting the heat and mass transfer process in the liquid desiccant dehumidifier. Renewable and Sustainable Energy Reviews 2014; 31: 587-599.
[17] Burns JR, Ramshaw C, Jachuck RJ. Measurement of liquid film thickness and the determination of spin-up radius on a rotating discussing an electrical resistance technique. Chemical Engineering Science 2003; 58: 2245-2253.
[18] Liu J, Liu XH, Zhang T. Performance comparison of three typical types of internally-cooled liquid desiccant dehumidifiers. Building and Environment 2016; 103: 134-145.
[19] Zhang T, Liu XH, Jiang JJ, Chang XM, Jiang Y. Experimental analysis of an internally-cooled liquid desiccant dehumidifier. Building and Environment 2013; 63: 1-10.
[20] Yin YG, Zhang XS, Wang G, Luo L. Experimental study on a new internally cooled/heated dehumidifier/regenerator of liquid desiccant systems. International Journal of Refrigeration 2008; 31(5): 857-886.
[21] Luo YM, Shao SQ, Xu HB, Tian CQ. Dehumidification performance of [EMIM]BF4. Applied Thermal Engineering. 2011; 31(14-15): 2772-2777.
[22] Luo YM, Shao SQ, Qin F, Tian CQ, Yang HX. Investigation of feasibility of ionic liquids used in solar liquid desiccant air conditioning system, Solar Energy 2012; 86: 2718-2724.
[23] Ren CQ. Corrections to the simple effectiveness-NTU method for counter-flow cooling towers and packed bed liquid desiccant-air contact systems. Int. J. Heat Mass Transfer 2008; 51: 237-245.
[24] Khan AY, Ball HD. Development of a generalized model for performance evaluation of packed-type liquid sorbent dehumidifiers and regenerators. ASHRAE Transfer 1992; 98: 525-533.
[25] Niu RP. Modelling and numerical simulation of dehumidifier using LiCl solution as the liquid desiccant. Proceedings of the international conference on electrical engineering and automatic control, Shandong, 2010.
[26] Liu XH, Qu KY, Jiang Y. Empirical correlations to predict the performance of the dehumidifier using liquid desiccant in heat and mass transfer. Renewable Energy 2006; 31:1627-1639.
[27] Park MS. Howell JR, Vliet GC, Peterson J. Numerical and experimental results for coupled heat and mass transfer between a desiccant film and air in cross-flow. Int. J. Heat Mass Transfer 1994; 37: 395-402.
[28] Kabova YO, Kuznetsov VV. Downward flow of a non-isothermal thin liquid film with variable viscosity. J. Appl. Mech. Techn. Phys. 2002; 43: 895-901.
[29] Joo SW, Davis SH, Bankoff SG. A mechanism for rivulet formation in heated falling films. J. Fluid Mech. 1996; 321: 279-298.
[30] Peng CSP, Howell JR. The performance of various types of regenerators for liquid desiccants. J. Solar Energy Eng. 1984; 106:133-141.
[31] Jain S, Dhar PL, Kaushik SC, Experimental studies on the dehumidifier and regenerator of a liquid desiccant cooling system. Appl. Thermal Eng. 2000; 20(3): 253-267.
[32] Zhang F, Zhang ZHB, Geng J. Study on shrinkage characteristics of heated falling liquid films. AIChE Journal 2005; 51(11): 2899-2907.
[33] Qi RH, Lu L, Yang HX, Qin F. Investigation on wetted area and film thickness for falling film liquid desiccant regeneration system. Applied Energy 2013; 112: 93-101.

[34] Conde MR. Properties of aqueous solutions of lithium and calcium chlorides: formulations for use in air conditioning equipment design. International Journal of Thermal Science 2004; 43: 367-382.
[35] Yin YG, Zhang XS, Peng DG, Li XW. Model validation and case study on internally cooled/heated dehumidifier/regenerator of liquid desiccant systems. International Journal of Thermal Sciences 2009; 48: 1664-1671.
[36] Yin YG. Study on the coupled characteristic of heat and mass transfer between air and desiccant in liquid desiccant dehumidification and regeneration. PhD thesis. Southeast University 2009.
[37] Benaman J. A systematic approach to uncertainty analysis for a distributed watershed model. Ph.D. Thesis, School of Civil and Environmental Engineering, Cornell University, Ithaca, N.Y. 2002.
[38] Young T. An essay on the cohesion of fluids, Philosophical Transactions of the Royal Society of London 1805; 95:65-87.
[39] Qi RH, Lu L. Energy consumption and optimization of internally cooled/heated liquid desiccant air-conditioning system: A case study in Hong Kong. Energy 2014; 73: 801-808.